Kinetic and Mechanistic Evaluation of Inorganic Arsenic Species Adsorption onto Humic Acid Grafted Magnetite Nanoparticles

Mamun Rashid[1], George E. Sterbinsky[2], Miguel Ángel Gracia Pinilla[3], Yong Cai[1], Kevin E. O'Shea[1*]

[1]*Department of Chemistry and Biochemistry, Florida International University, 11200 SW 8th Street, Miami, Florida, 33199*

[2]*Advanced Photon Source, Argonne National Laboratory, 9700 Cass Avenue, Argonne, IL 60439*

[3]*Universidad Autónoma de Nuevo León, UANL, Facultad de Ciencias Físico Matemáticas, Ciudad Universitaria, San Nicolás de los Garza, N.L., México 66455*

*Corresponding author.

E-mail address: osheak@fiu.edu (K.E. O'Shea)

Abstract

Humic acid coated magnetic iron oxide nanoparticles (HA-MNP) were synthesized, characterized, and studied for the removal of toxic inorganic arsenic species from aqueous media. The adsorption of As(III) and As(V) followed pseudo-second order kinetics and the observed data were accurately modeled employing Freundlich adsorption isotherm. Application of the Weber and Morris intraparticle diffusion model to the observed kinetic data suggest that the adsorption occurs in three distinct stages, fast, intermediate, and slow steps. We propose the initial stage is governed by surface association, followed by intraparticle diffusion of arsenic through the HA matrix and finally, chemical reaction or bonding between the arsenic species and HA functionality. The HA-MNP nano-adsorbent absorbs > 95% of the inorganic arsenic species with an absorption capacity of 12.2-12.6 mg/g from aqueous media and is effective under a variety of conditions. Post arsenic adsorption characterization of the nanoparticles suggests that As(III) binds with the carboxylate group of HA through a proposed ester type linkage while electrophilic reactions can occur between the nucleophilic functional groups present in HA and the electrophilic arsenic atom in As(V). The results obtained demonstrated that HA-MNP are robust and have promise for effective As (III) and As(V) remediation.

1. INTRODUCTION

Arsenic occurrence in aquatic environments is the result of natural and man-made sources. While arsenic is discharged by industrial processes and used in agricultural applications, water contamination by arsenic is most often the contribution of dissolution or leaching of solid phase arsenic contained within the rocks, soil and minerals into groundwater.[1–3] This class one carcinogen has already exerted severe negative consequences on the health of more than a hundred million people as poisoned by arsenic contaminated groundwater used for drinking, irrigation and other household purposes.[4–6] Bangladesh, India, China, Vietnam, Argentina, Pakistan, USA, Chile and Mexico are among the countries most affected by arsenic contaminated tubewells and aquifers with arsenic concentrations well above the maximum contamination limit of 10 µg/L set by WHO.[5] Geology, topography, temporal variability influence the water pH and redox potentials and thus affects arsenic solubility.[7,8] Arsenite, As(III) and arsenate, As(V) are the most common toxic forms of arsenic present in drinking water sources. The major species in the reducing environment of groundwater is the more mobile and more toxic arsenite.[9] Development and implementation of effective methods for the removal of arsenic species from drinking water sources are critical to ensure quality water for millions of people worldwide.

Humic substances (HS) in aquatic systems are derived from the breakdown of soil humus and aquatic plants through different biological and chemical processes.[10] Different molecular moieties and wide variety of organic functional groups of HS are responsible for its structural diversity and physico-chemical properties such as solubility and surface charge distribution.[11] The more hydrophobic, large molecular weight fraction of HS, commonly referred to as humic acid (HA) generally exhibits higher sorption and complexation

characteristics over other HS fractions.[12,13] Humic acid coated/modified adsorbents for the environment friendly remediation of different contaminants from water have been studied.[14–16] Here we report the use of humic acid grafted to iron oxide nanoparticles for the adsorption of highly toxic inorganic arsenic species from water.

Adsorption is one of the most effective methods for toxic species remediation from aqueous media as it can limit the mobility and bioavailability of potent toxins at relatively low cost and simple operation.[17] Use of nanoadsorbent is particularly attractive because engineered nanomaterials can be tailored for greater surface area and stronger binding capacities.[18] Professor Prashant V. Kamat et al. have made significant contributions in the synthesis and characterization of hybrid nanomaterials for environmental and energy related applications. [19–23] A number of his studies focused on the potential remediation/degradation of various environmental pollutants including arsenic by using the adsorptive and/or photocatalytic properties of the nanomaterials.[24–27]

Iron based nano-adsorbents have received tremendous attention due to the availability and low cost of the raw materials. The strong magnetic property of tailor-made iron particles is conducive for easy recovery and/or separation. Magnetite (Fe_3O_4) nanoparticles are among the most promising adsorbents with the advantages of superparamagnetic properties, easy preparation and bio-compatibility. However, agglomeration and the loss of magnetic strength over time resulting from auto-oxidations limits the commercial applications of bare iron oxide nanoparticles.[16] These constraints have been addressed using organic substrates to coat the surface of magnetite (Fe_3O_4) nanoparticles. The coating protects against auto-oxidation of the iron oxide core. Tremendous potential is observed for the environmental applications of magnetite nanoparticles coated with humic acid (HA), where the surface charge associated

with the nanoparticles is converted from positive to negative upon the appropriate coating of humic acid on magnetite.[28,29] The strong affinity of polyanionic humic acid to magnetite is found to be useful in coating the surface effectively which in effect significantly reduces or eliminates the nanotoxicity of bare magnetite nanoparticles (MNP) and enhances their chemical and colloidal stability.[30,31] The saturation magnetization of bare MNP and HA-MNP are reported to be 79.6 and 68.1 emu/g respectively, thus demonstrates the retention of strong magnetic property by the nanoparticles even after the coating of humic acid on the surface.[16] Liu et al. was the first to demonstrate the potential application of humic acid coated magnetite nanoparticles (HA-MNP) for the adsorption and removal of toxic metal cations.[16] Although the application of negatively charged HA-MNP materials for adsorption of toxic cations is effective due to electrostatic attractions between adsorbent surface and toxic cations involved, we recently reported the successful removal of anionic chromium and phosphate from water using HA-MNP.[32,33] The adsorption mechanisms for anionic species is not based on electrostatic interactions but rather likely through the formation of chemical bonds between the adsorbate and the different functional groups present in humic acid. The carboxylic, phenolic, amino, and sulfhydryl moieties of HA can act as a potential binding sites for the toxic arsenic species. In the solution pH range of 3 to 9, the charge neutral H_3AsO_3 is the dominant species of As(III) whereas for As(V), the negatively charged $H_2AsO_4^-$ and $HAsO_4^{2-}$ are the most prevalent forms.[34] Here we examined the removal of both As(III) and As(V) using HA-MNP. The detailed characterization of HA-MNP and As-HA-MNP provide fundamental information about the bonding and adsorption mechanisms of As (III) and As(V) to the humic acid materials which can be extended to understand the fate, transport, and bioavailability of As (III) and As(V) in the natural aqueous systems. The results demonstrate for the first time

that HA-NMPs are an effective nano-adsorbent for As(III) and As(V). The As adsorption is readily modeled and predictable which are critical to meet specific treatment objectives in real-life applications. The knowledge obtained from the study can help guide the improvement of water treatment methodologies using green materials.

2. EXPERIMENTAL SECTION

2.1. Materials. Ammonium hydroxide (29.2%), ferric chloride hexahydrate (98.8%), sodium arsenite and sodium arsenate dibasic heptahydrate (≥ 98%) were purchased from Fisher Scientific. Ferrous chloride tetrahydrate (≥ 99%) and humic acid sodium salt were purchased from Sigma Aldrich.

2.2. Synthesis and application of HA-MNP. The nanoparticles were synthesized using

3. co-precipitation reported elsewhere.[16] Summary of the synthesis procedure are given in the supporting information. The arsenic solution with the added nanoparticles were mixed in the 50 mL plastic bottle and agitated in the orbit shaker at 250 rpm (Lab line instrument Inc., model 3520). For the adsorption experiments, the initial solution pH of arsenic was adjusted by using 0.1M HCl and 0.1M NaOH and monitored by pH meter (Mettler Toledo, model: SevenEasy). The particles were separated from solution and residual arsenic concentration and speciation were measured employing a Perkin Elmar ICP-MS coupled with HPLC. Although handheld magnet provides effective separation of the treated nanoparticles, to comply with the requirement of the analytical facility and to conveniently handle large number of samples of small volume, 0.45 μm syringe filters were used to filter the arsenic solution before analyzing in LC-ICP-MS.

RESULTS AND DISCUSSION

3.1. Characterization: HA-MNP were subjected to detail characterization before and after the adsorption of As(III) and As(V) species. Details of the sample preparation and characterization techniques are provided in the supporting information. The newly synthesized HA-MNPs exhibited the established key features.[16,32,33] The FTIR spectra of HA-MNP (Figure S1) exhibits characteristic band at 1598 cm^{-1} indicative of the C=O stretching of carboxylate functionality present in HA, the red shift from typical carboxylate band (1700 cm^{-1}) is characteristic of a weaker C=O bond as the carbonyl oxygen complexes with the magnetite core.[33] The strong broad IR band at 3300-2700 cm^{-1} observed in the neat HA-MNP can be attributed to the presence of phenolic O-H and/or carboxylic acid groups of HA in HA-MNP. A significant reduction in the O-H signal is observed after the adsorption of As(III) and As(V), suggesting the formation of chemical bond between the O-H groups in the HA coating and the As species.

The TEM image of the HA-MNP (Figure 1a) illustrates a thin film coating of humic acid on the magnetite surface. The TEM measurements yield the average diameter of 10.6 nm for the synthesized HA-MNP with standard deviation of 3.5 (Figure S2). STEM-HAADF image of arsenic loaded HA-MNP is shown in Figure 1b. High resolution TEM image of the arsenic laden nanoparticles (Figure 1c) reveals the characteristic lattice fringe distance of the original HA-MNP as 3.0 Å and 4.9 Å corresponding to the (220) and (111) crystallographic planes of magnetite. This observation indicates that arsenic species does not significantly bind to or change the crystalline lattice of the iron oxide core material. Since the HA-MNP core is unchanged upon adsorption of arsenic, the humic acid shell appears to shield the magnetite core from the arsenic species, thus suggesting that adsorption occurs within the humic acid matrix. EDS spectra of the As-loaded HA-MNP confirms the presence of arsenic in the

nanoparticle surface (Figure 1d). The copper (Cu) and silicon (Si) peaks in the EDS spectra are from the grids which are made of copper with a thin film coating of silicon on top. The Raman spectra of HA-MNP (Figure 2) shows the characteristic magnetite bands at 535 and 668 cm^{-1} while the characteristic bands associated with maghemite at 350, 500 and 720 cm^{-1} are not observed.[35] With respect to the comparison of the Raman peaks at 220, 280, and 700 cm^{-1}, there is clearly variation in the relative proportion of these peaks. Such changes may be due to changes in the HA backbone or functionality upon binding of the arsenic species. Raman spectrum of the As(III)-HA-MNP (Figure 2) includes a band at 321 cm^{-1} which is assigned to the vibrational stretching of As(III)-O bond and a band at 357 cm^{-1} corresponds to the bending of O-As(V)-O bond.[36] While As(III) can be oxidized to As(V) by photochemical processes, great care was taken to eliminate light exposure of materials used in the experiments involving As(III). However, in an oxygen saturated environment in the presence of HA-MNP, conversion of As(III) to As(V) is observed (Figure S3) even in the absence of light. The HA-MNP promoted transformation of As(III) to As(V) under dark conditions could be initiated by trace metals in the HA materials and/or the presence of molecular oxygen.

The wide scan XPS spectra of HA-MNP (Figure S4a) shows the binding energy of approximately 285, 529 and 710 eV that corresponds to the photoelectron lines of C1s, O1s and Fe2p respectively.[37] Deconvolution of the peaks with corrected binding energy of adventitious carbon (284.8 eV) indicates the presence of C-C and C-H at 284.8 eV and the carboxylate group (COO^-) at 288.5 eV from HA, all pertaining to C1s (Figure S4b).[38,39] For O1s (Figure S4c), the two peaks at 528.8 and 531.4 eV can be ascribed to the anionic oxygen in magnetite and the oxygen containing functional groups of HA respectively.[39,40] In case of Fe2p spectra (Figure S4d), the $Fe2p_{3/2}$ peak at 708.9 and 710.6 eV are due to the presence of

Fe^{2+} and Fe^{3+} respectively while the peak at 724.1 is for $Fe2p_{1/2}$.[41] The peak at 740.3 eV corresponds to the $OKL_{23}L_{23}$ Auger lines of oxygen. The absence of the characteristic satellite peak of maghemite (γ-Fe_2O_3) at 719.0 eV further indicates that the coating of humic acid successfully inhibits the oxidation of magnetite core.[42] Iron K-edge XANES spectra and k^3 weighted EXAFS spectra of bare magnetite and HA-MNP are similar and consistent with the magnetite spectra reported in the literature [Figure S5(a & b)].[43] The arsenic K-edge XANES spectra of As(III) and As(V) loaded HA-MNP are shown in Figure S6. Although arsenic samples for XAS experiment were prepared in the nitrogen glovebox, partial conversion of As(III) to As(V) in the HA-MNP treated samples are observed (Figure S6a) whereas the XANES spectra of the adsorbed As(V) species remains largely unaffected (Figure S6b). The exposure of HA-MNP bound As(III) to molecular oxygen, the presence of trace metals in HA and/or the oxidizing environment of the beamline are assumed to play roles in the oxidation of HA-MNP adsorbed As(III) to As(V). At higher pH, As(III) is more readily converted to As(V) which may be related to pKa, change in speciation and susceptibility to oxidation. Linear combination fitting of Athena[44] was used to determine the percent conversion of As(III) to As(V) in As (III) loaded HA-MNP sample at neutral pH (Figure S7). As clearly observed from the figure, initially there was no As(V) species present in the sample meaning that the absence of molecular oxygen in the nitrogen glovebox inhibits the oxidation of As(III). However, with the exposure of the sample to the beamline, 25% of As(III) is converted to As(V) in 4.5 hours suggesting that the beam induced oxidation played a critical role in the conversion process.

3.2. Kinetics of Arsenic adsorption. The adsorption equilibrium and the corresponding uptake capacity for As(III) and As(V) of HA-MNP were determined to assess for their possible implementation. The adsorption experiments were run for three hours with samples collected

at pre-determined time intervals. The collected samples were filtered to separate the As-loaded HA-MNP from the solution and the filtrates analyzed by HPLC-ICP-MS to monitor the residual concentration of the As species in the solution. The results demonstrate As(V) is adsorbed by HA-MNP faster and to a greater extent than As(III). At a HA-MNP loading dose of 0.2 g/L and 200 ppb of the arsenic species, the level of As(III) can be reduced below the drinking water maximum contaminant level (MCL) of 10 ppb within 180 mins, while only 60 mins is required to reduce the concentration of As(V) below the MCL (Figure 3). Within one min of exposure to the HA-MNP, the initial concentrations of As(III) and As(V) are reduced by > 50 %. For an arsenic mixture of 200 ppb As(III) and 200 ppb As(V) (total initial arsenic concentration of 400 ppb), the complete removal of arsenic species was achieved at a dose of 0.2 g/L HA-MNP illustrated by Figure S8. Results from the competition study suggest that As(III) and As(V) might have some preferential sorption sites in HA surface of HA-MNP and so, the presence of one arsenic species did not appear to interfere significantly in the removal process of another. The difference in formal charge and the presence (or absence) of lone pair of electrons in the arsenic atom of the studied arsenic species has made them susceptible to attack by the two different classes of functional groups of HA with completely opposite characteristics.

Adsorption efficiency and the adsorption mechanisms were evaluated by fitting the experimental data into the Lagregren's pseudo-first order and Ho and McKay's pseudo-second order kinetic models.[45,46] The pseudo-first order model determines the sorption constant based on solid surface capacity while the pseudo-second order model works on solid phase sorption.[46] The full mathematical expressions of the two models are given in the supporting information. The kinetic parameters obtained from the application of the models to the experimental data

for As(III) and As(V) adsorption on HA-MNP are summarized in Table 1. For the pseudo-second order model, there is an excellent match observed between the experimental and calculated Q_e values. The high correlation coefficient (R^2) also indicates the best fitting of the adsorption process with the pseudo-second order model. This finding suggests that for the arsenic adsorption process, rate is proportional to the square of the number of available adsorption sites in the nanoparticles.[46,47] The kinetic data of arsenic adsorption was further investigated by using the Weber and Morris intraparticle diffusion model which when applied to the observed results shows that three distinct steps are associated with the adsorption process (Figure 4). We propose the first stage as the initial, rapid association of arsenic on the HA-MNP surface, second stage is the diffusion of arsenic species into the HA matrix of the nanoparticles and the final stage is the adsorbent-adsorbate chemical reaction/bonding that eventually lead to equilibrium. Overall, the adsorption of arsenic species on HA-MNP can be viewed as a complex, multi-step adsorbent-adsorbate interaction where sharing or exchange of electrons and bonding between the synthesized nanoparticles and the target arsenic species played critical roles in the observed behavior.

3.3. Adsorption Isotherms. The adsorption isotherms of individual arsenic species were measured as a function of initial arsenic concentration to investigate the interactions between solid surface and adsorbent relative to the aqueous solvation of arsenic. The initial arsenic concentration was varied from 0.1 to 10 mg/L at constant loading of HA-MNP (0.2 g/L). Data from the isotherm study were fitted in the Langmuir and Freundlich models to probe the adsorption mechanisms at the solid-liquid interface. The major differences between the two models are the assumptions about the surface characteristics and the mechanism of solute binding onto the adsorbent surface. The Langmuir model assumes homogeneous adsorbent

surface with a finite number of identical adsorption sites which can be occupied by only one target molecule leading to the formation of one uniform monolayer.[48,49] In contrast, differential adsorption is assumed in Freundlich model where multilayer adsorption can occur on heterogeneous adsorbent surface having different degrees of affinity for the adsorbate with stronger binding sites occupied first.[50] Based on the correlation coefficient for the Langmuir and Freundlich plots of the measured experimental data, the adsorption process is found more consistent with the Freundlich model indicative of the multilayer formation and/or heterogeneous adsorption surface sites of HA-MNP. The parameters from the Langmuir and Freundlich isotherms equation are presented in Table 2. From Freundlich model, the value of 1/n less than 1 is indicative of chemisorption of As(III) and As(V) on HA-MNP.[50] Although the relative adsorption capacity (K_f) is found to be slightly higher for As(III) than As(V) (2.96 vs 2.30), the much lower 1/n value of As(V) (0.28) supports its stronger adsorption intensity compared to As(III) (0.57). This is also evident from the kinetic data where faster and more extensive adsorption was observed for As(V) relative to As(III). The maximum adsorption capacities of HA-MNP measured under our experimental condition are 12.2 and 12.6 mg/g for As(III) and As(V) respectively. Similar types of coated and uncoated iron oxide adsorbents reported in the literature shows the maximum removal capacity for both As(III) and As(V) in the range of 5.27 to 16.63 mg/g.[34,37,51]. The competitive arsenic adsorption capacity of HA-MNP validates its strong potential to be used in real life arsenic treatment plants.

3.4. pH effect. The pH dependent adsorption and binding mechanisms of oxyanions are complicated by their speciation and the surface charge of the absorbent.[52,53] To probe the influence of solution pH, the initial pH of aqueous solutions of As(III) and As(V) was adjusted using 0.1 M NaOH and 0.1 M HCl. The adsorption of As(III) and As(V) on HA-MNP was

unchanged from pH 3 to 8 (Figure S9). But under highly alkaline conditions the adsorption of arsenic decreased. For As(III), at pH 8 & 10, adsorption (removal) was 96% and 78% respectively; for As(V) at the same pH, it was 98% and 70% respectively. While adsorption was reduced overall, the HA-MNP still exhibit significant adsorption of both As(III) and As(V) under highly alkaline conditions. The modest decrease in adsorption can be explained by formal and surface charges as a function of solution pH considering the pH_{pzc} of HA-MNP and the pKa values of the arsenic species. As(V) exists in monoanionic ($H_2AsO_4^-$) and dianionic ($HAsO_4^{2-}$) forms whereas As(III) mostly exists as a stable neutral hydroxo complex, $As(OH)_3$ over the range of solution pH studied. The HA-MNP is negatively charged at solution pH greater than its pH_{pzc} of 3.3.[32] Attractive electrostatic interactions are minimal or non-existent in binding the neutral As(III) on HA-MNP; for As(V) however, electrostatic repulsion between negatively charged sorbent and sorbate could inhibit adsorption at pH > 3.3. Despite the electrostatic repulsion, chemical reactions between the functional groups of humic acids and As(V) appear to be dominant in the adsorption process. The possible binding mechanisms for As(III) and As(V) can include ligand exchange and/or formation of adducts through esterification.[54] Decrease in the characteristic O-H group signal in IR spectra of the HA-MNP upon addition of As(III) and As(V) indicate the OH groups are critical and transformed upon exposure to arsenic consistent with the formation of ester-type bonds. Raman peaks in the As (III) laden materials also exhibit bands characteristic of ester or ether formation reactions between the OH group associated with the HA and the arsenic species. With this in mind, we proposed the following reaction mechanisms: for As(III), ester type linkages could form (equation 1) due to reaction between the carboxylate functional group in HA with the nucleophilic OH of As(III). Conversely, nucleophilic functional groups, such as phenolic -OH,

RSH, RCOO-, R-NH_2 can undergo addition type reactions with the electrophilic arsenic atom in As(V) (equation 2).[54]

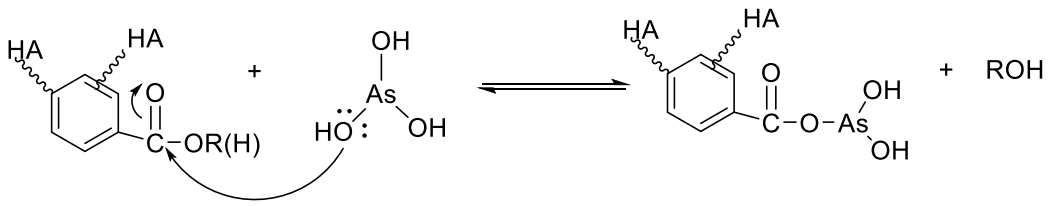

(1)

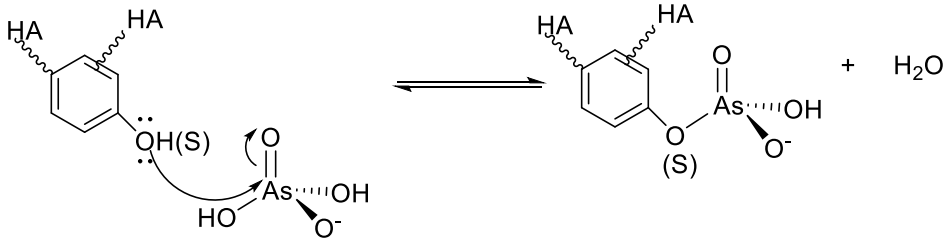

(2)

HA-MNP adsorption of As(V) is stronger and more extensive than As(III). The four oxygen atoms attached to the central As(V) can serve as chelating atoms or as nucleophiles in addition type reactions. The electronegativity of the oxygen atoms and pi bond also make the As(V) atom electrophilic and susceptible to accepting an electron pair or addition-elimination mechanisms such as addition of phenolate entity resulting in the formation of ester type functionalities.[54] The lone electron pair and sp^3 hybridization of As(III) make it unreactive as an electrophile. The lower reactivity of As(III) can reduce binding to HA-MNP as observed in the study.[55] Under strongly alkaline conditions (pH > 9) with solution pH above the pKas of the As(III) and As(V) species, the repulsion between the negatively charged As species and HA-MNP slows down the adsorption and/or ligand exchange processes. Also, the higher concentrations of hydroxide present under alkaline conditions may hydrolyze the ester linkages between the arsenic species and the hydroxyl groups associated with HA materials resulting in lower observed adsorption of the arsenic species on HA-MNP.

3.5. Influence of co-existing ions. The influence of different anions that commonly exist in natural waters contaminated with arsenic on HA-MNP adsorption were studied. The anions, SO_4^{2-}, CO_3^{2-}, PO_4^{3-}, Cl^- and NO_3^- were added individually at 1 mM to the specific adsorbent-adsorbate mixtures. Sulfate, chloride, and nitrate showed no inhibition on the adsorption of As(III) and As(V) shown in Figure S10. Phosphate exhibited modest competition for the adsorption sites leading to slight decreases in the adsorption of both As(III) and As(V) on HA-MNP. Arsenic and phosphorous are from group 15 of the periodic table and share some structural and chemical similarities.[56] Arsenic and phosphorous thus can exhibit analogous adsorption and chelating properties in competing for adsorption onto HA-MNP sites. However, in natural water systems, the mass ratio of phosphate to arsenic is generally quite low and not a concern in most cases.[57] Carbonate showed modest inhibition of the adsorption of As(V) species. The addition of carbonate to As(III) and As(V) solutions results in an alkaline solution, pH ≈ 9. Under these conditions, As(III) exist predominantly as a neutral species while As(V) exists in the dianionic form and the strong repulsion with HA-MNP can reduce the uptake of As(V). In a separate study, we have also investigated the effect of iron presence in the adsorption process since arsenic and iron commonly co-exists under similar geochemical environment in the aqueous system. Analysis of the residual arsenic concentration showed that (Table S1) more than 97% of the arsenic species were adsorbed on HA-MNP surface which means iron does not exhibit any interference or compete with the arsenic species for the binding sites of the nanoparticles. In summary, most common ions had minimal influence on the adsorption of As(III) and As(V) under the neutral pH conditions encountered in natural water systems.

3.6. Release of humic acid and As desorption study. The presence of humic

materials can interfere with water treatment processes and lead to disinfection byproduct (DBP) formation. Leaching of humic acid from HA-MNP or presence of free HA in solution can compete for the adsorption of the arsenic species, which is undesirable since As bound to free HA will not be removed during the magnetic collection of As laden HA-MNP.[58] Loss of HA from the surface of the nanoparticle can also increase the exposure of the magnetite core to the ambient environment and subsequent oxidation. To determine the amount of humic material leached from HA-MNP upon adsorption of arsenic, batch experiments were carried out. 0.05 g of HA-MNP was separately loaded in 50 mL of water (control), As(III) and As(V) solutions with pH adjusted to 6.6 ± 0.1. The reaction was carried out at room temperature for a total of three hours. After separation of the HA-MNP, the concentration of DOM in the resulting solution measured by TOC analysis was used to determine the free humic acid in different samples. The DOM concentrations regardless of the presence of As(III) or As(V) is between 0.25 and 0.57 mg/L (Table S2), which is within the typical concentration of NOM found in the aquatic environments.[59] The result demonstrates the stability and robustness of the synthesized nanoparticles. Desorption study was carried out by treating the arsenic adsorbed nanoparticles with H_2O_2 and HNO_3 at 110 °C for 90 minutes. The mass balance calculation of total arsenic showed that more than 99% (data not shown) of the adsorbed species can be successfully recovered from the HA-MNP surface.

4. CONCLUSIONS

The environmentally friendly, magnetic adsorbent HA-MNP has been found consistently effective for the removal of As(III) and As(V) under different environmental conditions. Study indicates the adsorption of As(III) and As(V) occurs in three different stages within the

functionality of the HA coating via surface association, intraparticle diffusion and complexation reactions or ligand exchange. Presence of characteristic bands of As(III)-O and O-As(V)-O in the Raman spectra of arsenic loaded HA-MNP, fitting of the kinetic data into the pseudo-second order model and Freundlich isotherm, pattern/efficiency of binding of As(III) and As(V) on HA-MNP at different pH- all suggest that chemisorption played the major role in the arsenic species removal process using HA-MNP. TEM, FTIR, XAS and TOC analysis of the synthesized HA-MNP after arsenic adsorption shows that the magnetite core remains unaffected throughout the process, thus confirming the robust nature of HA coating that perfectly shields the magnetite core of the nanoaprticles. The successful arsenic remediation process with detailed characterizations and mechanistic insights presented in the paper can be an important layout for the design and development of a sustainable water treatment technology.

ASSOCIATED CONTENT

Supporting Information

Details of experimental procedure and sample preparation; characterization of the synthesized HA-MNP before and after arsenic adsorption under different environmental conditions, effect of iron during arsenic adsorption onto HA-MNP and DOC release information.

AUTHOR INFORMATION

Corresponding Author

*Email: osheak@fiu.edu. (Kevin E. O'Shea). Tel: +1 305 3483968. Fax: +1 305 3483772

Notes

The authors declare no competing financial interest.

ACKNOWLEDGEMENTS

We dedicate this paper to the tremendous contributions Professor Prashant Kamat has made to the fundamental understanding of interfacial processes and advancement of nanoscience. It has been distinct honor to collaborate with Professor Phashant Kamat for more than 20 years. This research used resources of the Advanced Photon Source, a U.S. Department of Energy (DOE) Office of Science User Facility operated for the DOE Office of Science by Argonne National Laboratory (ANL) under Contract No. DE-AC02-06CH11357. We thank Richard Rosenberg of Advanced Photon Source of ANL for his kind assistance with the XPS measurement of the samples. We also appreciate the help of Shamima Nasreen, Peter Kerns and the Suib research group surface analysis lab of UConn for their help in analyzing the XPS data using Casa XPS software. The authors gratefully acknowledge NSF program (ECS1710111) for the support in the work.

References

(1) Amini, M.; Abbaspour, K. C.; Berg, M.; Winkel, L.; Hug, S. J.; Hoehn, E.; Yang, H.; Johnson, C. A. Statistical Modeling of Global Geogenic Arsenic Contamination in Groundwater. *Environ. Sci. Technol.* **2008**, *42* (10).

(2) Zheng, S.; Jiang, W.; Rashid, M.; Cai, Y.; Dionysiou, D. D.; O'Shea, K. E. Selective Reduction of Cr(VI) in Chromium, Copper and Arsenic (CCA) Mixed Waste Streams Using UV/TiO2 Photocatalysis. *Molecules* **2015**, *20* (2), 2622–2635.

(3) Mondal, P.; Bhowmick, S.; Jullok, N.; Ye, W.; Van Renterghem, W.; Van Den Berghe, S.; Van Der Bruggen, B. Behavior of As(V) with ZVI-H2O System and the Reduction to As(0). *J. Phys. Chem. C* **2014**, *118* (37), 21614–21621.

(4) Brammer, H.; Ravenscroft, P. Arsenic in Groundwater: A Threat to Sustainable Agriculture in South and South-East Asia. *Environ. Int.* **2009**, *35* (3), 647–654.

(5) Rahman, S.; Kim, K. H.; Saha, S. K.; Swaraz, A. M.; Paul, D. K. Review of Remediation Techniques for Arsenic (As) Contamination: Anovel Approach Utilizing Bio-Organisms. *J. Environ. Manage.* **2014**, *134*, 175–185.

(6) Yan, W.; Ramos, M. A. V; Koel, B. E.; Zhang, W. X. As(III) Sequestration by Iron Nanoparticles: Study of Solid-Phase Redox Transformations with X-Ray Photoelectron Spectroscopy. *J. Phys. Chem. C* **2012**, *116* (9), 5303–5311.

(7) Buschmann, J.; Berg, M.; Stengel, C.; Sampson, M. L. Arsenic and Manganese Contamination of Drinking Water Resources in Cambodia: Coincidence of Risk Areas with Low Relief Topography. *Environ. Sci. Technol.* **2007**, *41* (7), 2146–2152.

(8) Fendorf, S.; Michael, H. A.; van Geen, A. Spatial and Temporal Variations of Groundwater Arsenic in South and Southeast Asia. *Science (80-.).* **2010**, *328* (5982), 1123–1127.

(9) Yu, L.; Peng, X.; Ni, F.; Li, J.; Wang, D.; Luan, Z. Arsenite Removal from Aqueous Solutions by □ -Fe 2 O 3 – TiO 2 Magnetic Nanoparticles through Simultaneous Photocatalytic Oxidation and Adsorption. *J. Hazard. Mater.* **2013**, *246–247*, 10–17.

(10) Thurman, E. M.; Malcolm, R. L. Preparative Isolation of Aquatic Humic Substances. *Environ. Sci. Technol.* **1981**, *15* (4), 463–466.

(11) Cook, R. L.; Langford, C. H. Structural Characterization of a Fulvic Acid and a Humic Acid Using Solid-State Ramp-CP-MAS 13 C Nuclear Magnetic Resonance. *Environ. Sci. Technol.* **1998**, *32* (5), 719–725.

(12) Meier, M.; Namjesnik-Dejanovic, K.; Maurice, P. A.; Chin, Y. P.; Aiken, G. R. Fractionation of Aquatic Natural Organic Matter upon Sorption to Goethite and Kaolinite. *Chem. Geol.* **1999**, *157* (3–4), 275–284.

(13) De Paolis, F.; Kukkonen, J. Binding of Organic Pollutants to Humis and Fulvic Acids: Influence of pH and the Structura of Humis Material. *Chemosphere* **1997**, *34* (8), 1693–1704.

(14) Yang, K.; Xing, B. Sorption of Phenanthrene by Humic Acid-Coated Nanosized TiO 2 and ZnO. *Environ. Sci. Technol.* **2009**, *43* (6), 1845–1851.

(15) Wu, P.; Zhang, Q.; Dai, Y.; Zhu, N.; Dang, Z.; Li, P.; Wu, J.; Wang, X. Adsorption of Cu(II), Cd(II) and Cr(III) Ions from Aqueous Solutions on Humic Acid Modified Ca-Montmorillonite. *Geoderma* **2011**, *164* (3–4), 215–219.

(16) Liu, J.; Zhao, Z.; Jiang, G. Coating Fe 3 O 4 Magnetic Nanoparticles with Humic Acid for High Efficient Removal of Heavy Metals in Water. *Environ. Sci. Technol.* **2008**, *42* (18), 6949–6954.

(17) Chang, F.; Qu, J.; Liu, R. Practical Performance and Its E Ffi Ciency of Arsenic Removal from Groundwater Using Fe-Mn Binary Oxide. *J. Environ. Sci.* **2010**, *22* (1), 1–6.

(18) Kurniawan, T. A.; Sillanpää, M. E. T.; Sillanpää, M. Nanoadsorbents for Remediation of Aquatic Environment: Local and Practical Solutions for Global Water Pollution Problems. *Crit. Rev. Environ. Sci. Technol.* **2012**, *42* (12), 1233–1295.

(19) Seger, B.; Kamat, P. V. Electrocatalytically Active Graphene-Platinum Nanocomposites .

Role of 2-D Carbon Support in PEM Fuel Cells Electrocatalytically Active Graphene-Platinum Nanocomposites . Role of 2-D Carbon Support in PEM Fuel Cells. **2009**, 7990–7995.

(20) Muszynski, R.; Seger, B.; Kamat, P. V. Decorating Graphene Sheets with Gold Nanoparticles. *J. Phys. Chem. C* **2008**, *112* (14), 5263–5266.

(21) Kamat, P. V. Photophysical, Photochemical and Photocatalytic Aspects of Metal Nanoparticles. *J. Phys. Chem. B* **2002**, *106* (32), 7729–7744.

(22) Pernik, D. R.; Tvrdy, K.; Radich, J. G.; Kamat, P. V. Tracking the Adsorption and Electron Injection Rates of CdSe Quantum Dots on TiO2: Linked versus Direct Attachment. *J. Phys. Chem. C* **2011**, *115* (27), 13511–13519.

(23) Stamplecoskie, K. G.; Kamat, P. V. Synergistic Effects in the Coupling of Plasmon Resonance of Metal Nanoparticles with Excited Gold Clusters. *J. Phys. Chem. Lett.* **2015**, *6* (10), 1870–1875.

(24) Vinodgopal, K.; Wynkoop, D. E.; Kamat, P. V. Environmental Photochemistry on Semiconductor Surfaces: Photosensitized Degradation of a Textile Azo Dye, Acid Orange 7, on TiO2 Particles Using Visible Light. *Environ. Sci. Technol.* **1996**, *30* (5), 1660–1666.

(25) Vinodgopal, K.; Hotchandani, S.; Kamat, P. V. Electrochemically Assisted Photocatalysis: Titania Particulate Film Electrodes for Photocatalytic Degradation of 4-Chlorophenol. *J. Phys. Chem.* **1993**, *97* (35), 9040–9044.

(26) Xu, T.; Kamat, P. V.; Joshi, S.; Mebel, A. M.; Cai, Y.; O'Shea, K. E. Hydroxyl Radical Mediated Degradation of Phenylarsonic Acid. *J. Phys. Chem. A* **2007**, *111* (32), 7819–7824.

(27) Xu, T.; Kamat, P. V.; O'Shea, K. E. Mechanistic Evaluation of Arsenite Oxidation in TiO 2 Assisted Photocatalysis. *J. Phys. Chem. A* **2005**, *109* (40), 9070–9075.

(28) Illés, E.; Tombácz, E. The Effect of Humic Acid Adsorption on pH-Dependent Surface Charging and Aggregation of Magnetite Nanoparticles. *J. Colloid Interface Sci.* **2006**, *295* (1), 115–123.

(29) Tombácz, E.; Tóth, I. Y.; Nesztor, D.; Illés, E.; Hajdú, A.; Szekeres, M.; L.Vékás. Adsorption of Organic Acids on Magnetite Nanoparticles, pH-Dependent Colloidal Stability and Salt Tolerance. *Colloids Surfaces A Physicochem. Eng. Asp.* **2013**, *435*, 91–96.

(30) Peng, L.; Qin, P.; Lei, M.; Zeng, Q.; Song, H.; Yang, J.; Shao, J.; Liao, B.; Gu, J. Modifying Fe 3O 4 Nanoparticles with Humic Acid for Removal of Rhodamine B in Water. *J. Hazard. Mater.* **2012**, *209–210*, 193–198.

(31) Illés, E.; Tombácz, E. The Role of Variable Surface Charge and Surface Complexation in the Adsorption of Humic Acid on Magnetite. *Colloids Surfaces A Physicochem. Eng. Asp.* **2003**, *230* (1–3), 99–109.

(32) Jiang, W.; Cai, Q.; Xu, W.; Yang, M.; Cai, Y.; Dionysiou, D. D.; O'Shea, K. E. Cr(VI) Adsorption and Reduction by Humic Acid Coated on Magnetite. *Environ. Sci. Technol.* **2014**, *48* (14), 8078–8085.

(33) Rashid, M.; Price, N. T.; Gracia Pinilla, M. ?ngel; O'Shea, K. E. Effective Removal of Phosphate from Aqueous Solution Using Humic Acid Coated Magnetite Nanoparticles. *Water Res.* **2017**, *123*, 353–360.

(34) Liu, C. H.; Chuang, Y. H.; Chen, T. Y.; Tian, Y.; Li, H.; Wang, M. K.; Zhang, W. Mechanism of Arsenic Adsorption on Magnetite Nanoparticles from Water: Thermodynamic and Spectroscopic Studies. *Environ. Sci. Technol.* **2015**, *49* (13).

(35) Daou, T. J.; Pourroy, G.; Bégin-Colin, S.; Grenèche, J. M.; Ulhaq-Bouillet, C.; Legaré, P.; Bernhardt, P.; Leuvrey, C.; Rogez, G. Hydrothermal Synthesis of Monodisperse Magnetite Nanoparticles. *Chem. Mater.* **2006**, *18* (18), 4399–4404.

(36) Goldberg, S.; Johnston, C. T. Mechanisms of Arsenic Adsorption on Amorphous Oxides Evaluated Using Macroscopic Measurements, Vibrational Spectroscopy, and Surface Complexation Modeling. *J. Colloid Interface Sci.* **2001**, *234* (1), 204–216.

(37) Chandra, V.; Park, J.; Chun, Y.; Lee, J. W.; Hwang, I.; Kim, K. S. Removal. **2010**, *4* (7), 2005–2009.

(38) Yang, D.; Velamakanni, A.; Bozoklu, G.; Park, S.; Stoller, M.; Piner, R. D.; Stankovich, S.; Jung, I.; Field, D. A.; Ventrice, C. A.; et al. Chemical Analysis of Graphene Oxide Films after Heat and Chemical Treatments by X-Ray Photoelectron and Micro-Raman Spectroscopy. *Carbon N. Y.* **2009**, *47* (1), 145–152.

(39) Wilson, D.; Langell, M. A. XPS Analysis of Oleylamine/oleic Acid Capped Fe3O4 Nanoparticles as a Function of Temperature. *Appl. Surf. Sci.* **2014**, *303*, 6–13.

(40) Lin, T. C.; Seshadri, G.; Kelber, J. A. A Consistent Method for Quantitative XPS Peak Analysis of Thin Oxide Films on Clean Polycrystalline Iron Surfaces. *Appl. Surf. Sci.* **1997**, *119*, 83–92.

(41) Grosvenor, A. P.; Kobe, B. A.; Biesinger, M. C.; McIntyre, N. S. Investigation of Multiplet Splitting of Fe 2p XPS Spectra and Bonding in Iron Compounds. *Surf. Interface Anal.* **2004**, *36* (12), 1564–1574.

(42) Zhang, D.; Liu, Z.; Han, S.; Li, C.; Lei, B.; Stewart, M. P.; Tour, J. M.; Zhou, C. Magnetite (Fe 3O 4) Core-Shell Nanowires: Synthesis and Magnetoresistance. *Nano Lett.* **2004**, *4* (11), 2151–2155.

(43) Sun, Y.; Guan, X.; Wang, J.; Meng, X.; Xu, C.; Zhou, G. E Ff Ect of Weak Magnetic Field on Arsenate and Arsenite Removal from Water by Zerovalent Iron: An XAFS Investigation. **2014**.

(44) Ravel, B.; Newville, M. ATHENA, ARTEMIS, HEPHAESTUS: Data Analysis for X-Ray Absorption Spectroscopy Using IFEFFIT. *J. Synchrotron Radiat.* **2005**, *12* (4), 537–541.

(45) Tseng, R. L.; Wu, F. C.; Juang, R. S. Characteristics and Applications of the Lagergren's First-Order Equation for Adsorption Kinetics. *J. Taiwan Inst. Chem. Eng.* **2010**, *41* (6), 661–669.

(46) Ho, Y. S.; McKay, G. Pseudo-Second Order Model for Sorption Processes. *Process Biochem.* **1999**, *34* (5), 451–465.

(47) Chen, R.; Zhi, C.; Yang, H.; Bando, Y.; Zhang, Z.; Sugiur, N.; Golberg, D. Arsenic (V) Adsorption on Fe3O4 Nanoparticle-Coated Boron Nitride Nanotubes. *J. Colloid Interface Sci.* **2011**, *359* (1), 261–268.

(48) Allen, S. J.; Mckay, G.; Porter, J. F. Adsorption Isotherm Models for Basic Dye Adsorption by Peat in Single and Binary Component Systems. *J. Colloid Interface Sci.* **2004**, *280* (2), 322–333.

(49) Mishra, A. K.; Ramaprabhu, S. Magnetite Decorated Multiwalled Carbon Nanotube Based Supercapacitor for Arsenic Removal and Desalination of Seawater. *J. Phys. Chem. C* **2010**, *114* (6), 2583–2590.

(50) Foo, K.Y.; Hameed, B. H. Insights into the Modeling of Adsorption Isotherm Systems. *Chem. Eng. J.* **2010**, *156*, 2–10.

(51) Lan, J. Removal of Arsenic from Aqueous Systems by Use of Magnetic Fe3O4@TiO2 Nanoparticles. *Res. Chem. Intermed.* **2015**, *41* (6), 3531–3541.

(52) He, G.; Zhang, M.; Pan, G. Influence of pH on Initial Concentration Effect of Arsenate Adsorption on TiO2 Surfaces: Thermodynamic, DFT, and EXAFS Interpretations. *J. Phys. Chem. C* **2009**, *113* (52), 21679–21686.

(53) Liang, Q.; Starr, K.; Zhao, D.; Feng, Y. Sorption of Arsenate by Polysaccharide-Stabilized Magnetite Nanoparticles: Effects of Stabilizers and Water Chemistry. *Abstr. Pap. 239th ACS Natl. Meet. San Fr. CA, United States, March 21-25, 2010* **2012**, No. C, IEC-53.

(54) Buschmann, J.; Kappeler, A.; Lindauer, U.; Kistler, D.; Berg, M.; Sigg, L. Arsenite and Arsenate Binding to Dissolved Humic Acids: Influence of pH, Type of Humic Acid, and Aluminum. *Environ. Sci. Technol.* **2006**, *40* (19), 6015–6020.

(55) Ren, J.; Fan, W.; Wang, X.; Ma, Q.; Li, X.; Xu, Z.; Wei, C. In Fl Uences of Size-Fractionated Humic Acids on Arsenite and Arsenate Complexation and Toxicity to Daphnia Magna. *Water Res.* **2017**, *108*, 68–77.

(56) Paul, B.; Parashar, V.; Mishra, A.; Mukherjee, A.; Sengupta, M. K.; Hossain, M. A.; Ahamed, S.; Das, B.; Nayak, B.; Lodh, D.; et al. Graphene in the Fe 3 O 4 Nano-Composite Switching the Negative Influence of Humic Acid Coating into an Enhancing Effect in the Removal of Arsenic from Water. *Environ. Sci. Water Res. Technol.* **2015**, *1* (1), 77–83.

(57) Li, J.; Wu, Y. N.; Li, Z.; Zhang, B.; Zhu, M.; Hu, X.; Zhang, Y.; Li, F. Zeolitic Imidazolate Framework-8 with High Efficiency in Trace Arsenate Adsorption and Removal from Water. *J. Phys. Chem. C* **2014**, *118* (47), 27382–27387.

(58) Wang, S.; Mulligan, C. N. Effect of Natural Organic Matter on Arsenic Release from Soils and Sediments into Groundwater. *Environ. Geochem. Health* **2006**, *28* (3), 197–214.

(59) Jin, Y.; Liu, F.; Tong, M.; Hou, Y. Removal of Arsenate by Cetyltrimethylammonium Bromide Modified Magnetic Nanoparticles. *J. Hazard. Mater.* **2012**, *227–228* (C), 46–468.

Tables & Figures

Table 1. Kinetic parameters for the adsorption of arsenic onto HA-MNP

		Pseudo-first order kinetics			**Pseudo-second order kinetics**		
C_0 (0.2 mg/L)	Qe, expt. (mg/g)	Qe, calc. (mg/g)	k_1 (min^{-1})	R^2	Qe, calc. (mg/g)	k_2 (g $mg^{-1}min^{-1}$)	R^2
As(III)	0.96	0.30	0.02 ± 0.001	0.98	0.96	0.35 ± 0.02	0.99
As(V)	0.98	0.17	0.04 ± 0.003	0.93	0.99	1.31 ± 0.09	0.99

Table 2. Adsorption isotherm parameters for the binding of As(III) and As(V) onto HA-MNP

	Langmuir isotherm			**Freundlich isotherm**		
Species	Q_{max} (mg/g)	b (L/mg)	R^2	K_f	1/n	R^2
As(III)	12.2	3.46	0.96	2.96	0.57	0.99
As(V)	12.6	4.88	0.94	2.30	0.28	0.99

List of Figures:

Figure 1: (a) Low resolution TEM image of HA-MNP (b) STEM-HAADF image of As(III)-HA-MNP (c) HRTEM image of As(III)-HA-MNP and (d) EDS spectra of As(III)-HA-MNP

Figure 2: Raman spectra of HA-MNP and As(III)-HA-MNP

Figure 3: Comparison of adsorption kinetics of As(III) and As(V) on HA-MNP $[As(III)]_0$ = 200 ppb, $[As(V)]_0$ = 200 ppb, pH = 6.6, HA-MNP dose = 0.2 g/L, temperature = 25 °C

Figure 4: Weber-Morris intraparticle diffusion plot of As(III) and As(V) adsorption kinetic data. $[As(III)]_0$ = 200 ppb, $[As(V)]_0$ = 200 ppb, pH = 6.6, HA-MNP dose = 0.2 g/L, temperature = 25 °C

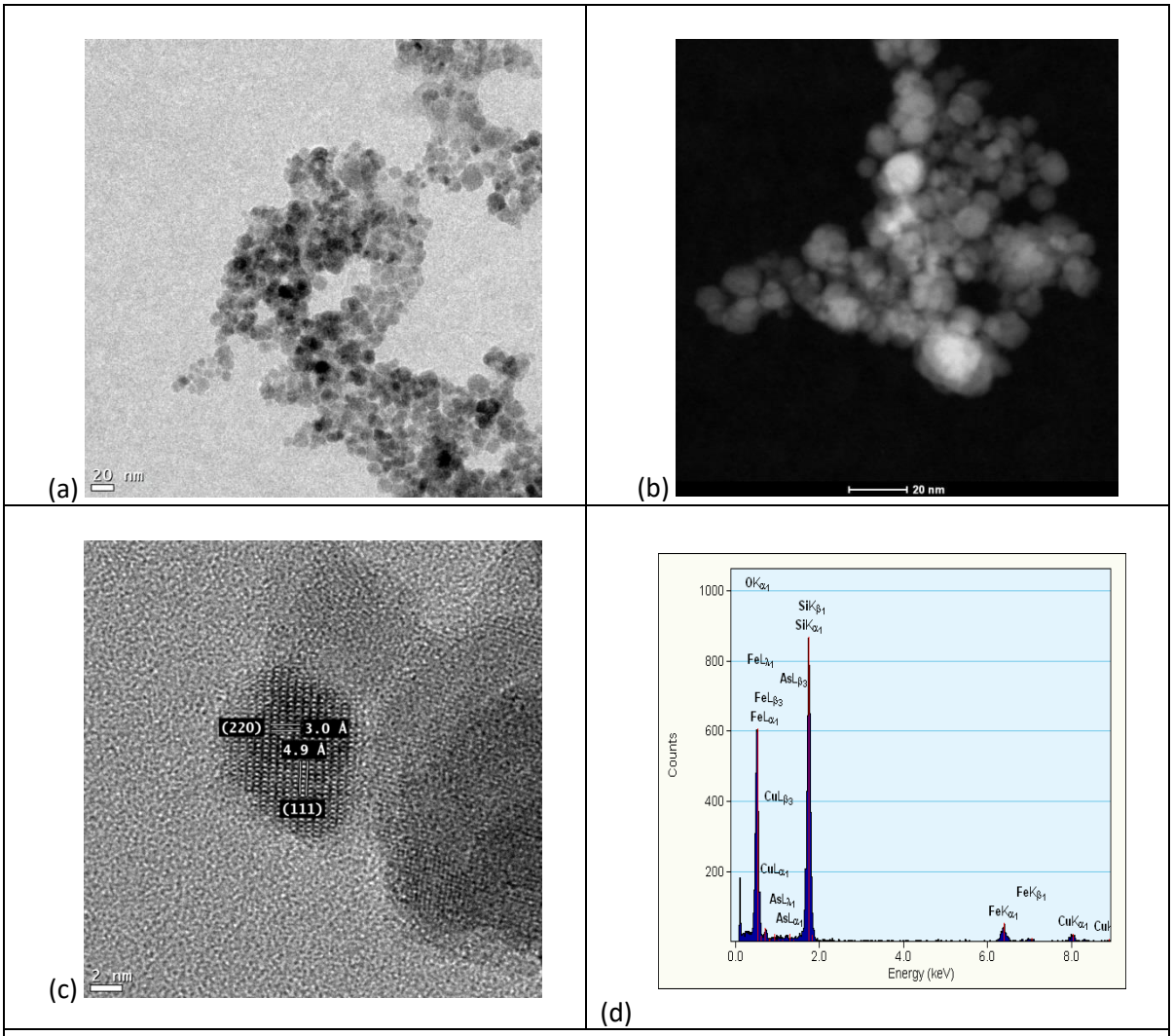

Figure 1: (a) Low resolution TEM image of HA-MNP (b) STEM-HAADF image of As(III)-HA-MNP (c) HRTEM image of As(III)-HA-MNP and (d) EDS spectra of As(III)-HA-MNP

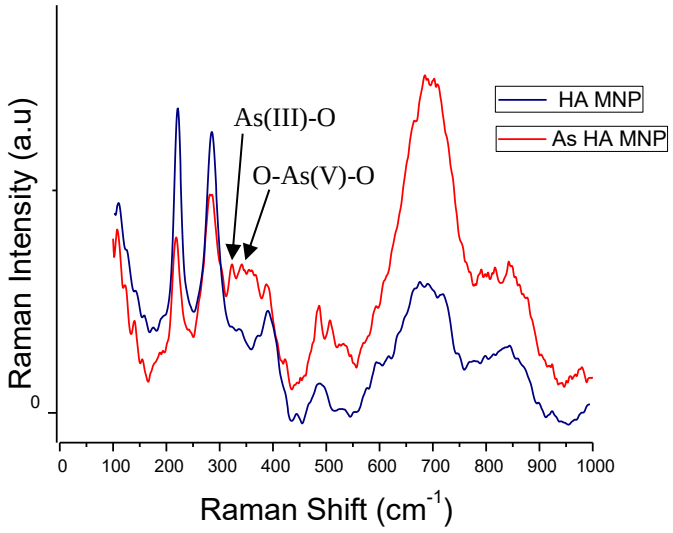

Figure 2: Raman spectra of HA-MNP and As(III)-HA-MNP

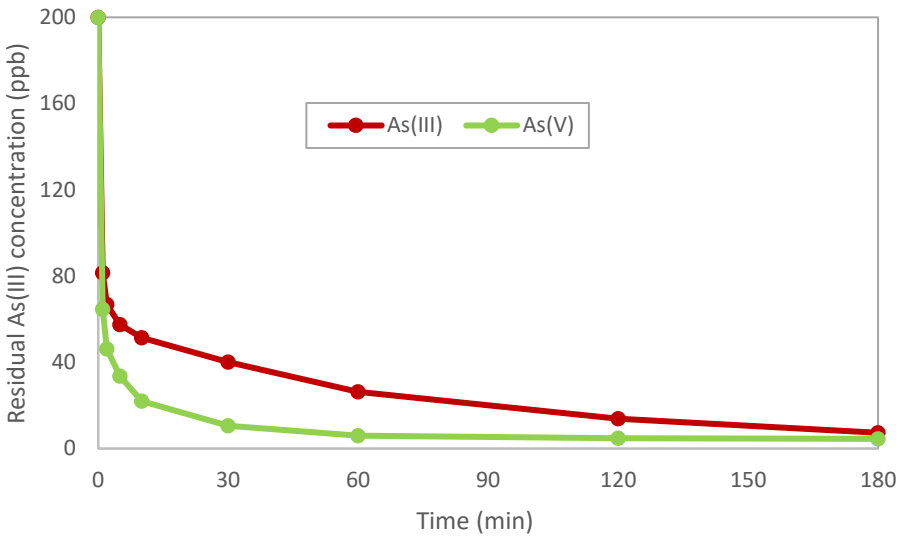

Figure 3: Comparison of adsorption kinetics of As(III) and As(V) on HA-MNP. $[As(III)]_0$ = 200 ppb, $[As(V)]_0$ = 200 ppb, pH = 6.6, HA-MNP dose = 0.2 g/L, temperature = 25 °C

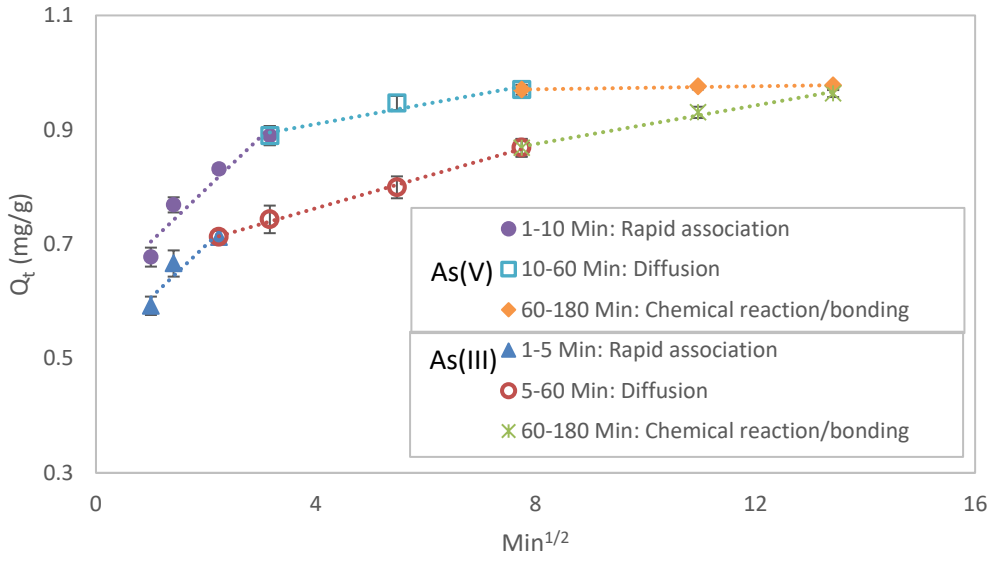

Figure 4: Weber-Morris intraparticle diffusion plot of As(III) and As(V) adsorption kinetic data. $[As(III)]_0$ = 200 ppb, $[As(V)]_0$ = 200 ppb, pH = 6.6, HA-MNP dose = 0.2 g/L, temperature = 25 °C